Transient kinetics and mechanism of oxygen adsorption over oxide catalysts from the TAP-reactor system

E.V. Kondratenko *, O.V. Buyevskaya **, M. Soick and M. Baerns

Institute for Applied Chemistry Berlin-Adlershof, Richard-Willstätter-Strasse 12, D-12489 Berlin, Germany
E-mail: ovb@aca-berlin.de

Received 25 May 1999; accepted 28 September 1999

For elucidating the mechanism of oxygen adsorption and its effect on selectivity in the oxidative coupling of methane (OCM) transient experiments were carried out in the TAP-2 reactor by pulsing oxygen over Na_2O/CaO catalysts at temperatures between 623 and 873 K. The response signals were fitted to three different models for oxygen adsorption. Model discrimination showed that only a reversible and dissociative adsorption via the molecular precursor provides a good description of the transient oxygen responses over all catalysts studied. Rate constants and activation energies of the elementary reaction steps of oxygen adsorption, desorption, dissociation and association were estimated. Doping CaO with sodium oxide influenced the ratio of k_{ads}/k_{dis} determining the coverage of the catalyst surface with molecular and atomic oxygen. The steady-state surface coverages with molecular and atomic adsorbed oxygen species were simulated for different partial oxygen pressures (0.5–15 kPa) using the kinetic parameters from transient experiments. These results may, however, be affected by extrapolating the pressure from 10^{-4} Pa to 15 kPa. It was derived that an increase of C_2 selectivity in OCM on Na_2O/CaO can be ascribed to a decrease in the coverages of adsorbed molecular oxygen, which appears to be a plausible interpretation confirming previous findings of the dependence of C_2 selectivity on oxygen partial pressure.

Keywords: temporal analysis of products (TAP) reactor, mathematical modelling of oxygen adsorption, estimation of kinetic parameters, oxidative coupling of methane

1. Introduction

The heterogeneous oxidation of light alkanes involves the activation of both hydrocarbon and the oxidant; the latter is an important step determining in many cases the selective pathway of the catalytic reactions [1–4]. In recent years different techniques such as temperature-programmed desorption (TPD) [5], Raman and IR spectroscopy [6], electron spin resonance (ESR) [7], work function measurements [8] and isotopic switching [9] have been used to study the interaction of oxygen with catalyst surfaces. Since the early work of Gleaves et al. [10] the "temporal analysis of products" (TAP) reactor was successfully applied for studying mechanistic aspects of solid-catalysed reactions [11–14]. By modelling the various processes (adsorption, desorption, reaction) occurring in the TAP reactor kinetic informations on surface processes were extracted from the response signals [15–19].

The aim of the present study was to determine kinetic parameters for elementary reaction steps occurring during the interaction of the gaseous oxygen with catalytic surfaces of doped and undoped CaO using the TAP-2 reactor and the programme described elsewhere [18,20]. Kinetic parameters derived from the transient experiments were used to simulate the surface steady-state coverages with molecular and atomic adsorbed oxygen for $p(O_2) = 0.5$–15 kPa in the absence of methane. Kinetic data obtained on Na_2O/CaO catalysts are discussed in terms of their influence on the selectivity of the oxidative coupling of methane (OCM).

2. Experimental

2.1. Catalysts

Na_2O/CaO catalysts were prepared from $CaCO_3$ (Alfa) and $NaHCO_3$ (Merck). $CaCO_3$ was calcined at 1273 K for 10 h to decompose the carbonate. After calcination the calcium oxide was impregnated with an aqueous solution of $NaHCO_3$ followed by drying at 400 K for 2 h and calcination at 1273 K for 2 h. After calcination the actual sodium concentration was determined by ICP-OES (inductively coupled plasma optical emission spectroscopy). The concentration of sodium is put inside brackets in the catalyst formula: Na(0.001 at%)/CaO, Na(1.2 at%)/CaO and Na(6.4 at%)/CaO.

The BET surface areas of the catalysts amounted to 6.3 $m^2\,g^{-1}$ for Na(0.001 at%)/CaO, 2.9 $m^2\,g^{-1}$ for Na(1.2 at%)/CaO and 2 $m^2\,g^{-1}$ for Na(6.4 at%)/CaO.

2.2. TAP measurements

The TAP-2 reactor system has been described in detail elsewhere [21]. The catalyst (100 mg; $d_p = 250$–355 μm) was packed between two layers of quartz of the same particle size in the reactor. Before each experiment the cata-

* Permanent address: Institute of Chemistry and Chemical Technology, Karl Marx ul. 42, Krasnoyarsk 660049, Russia
** To whom correspondence should be addressed.

lyst was treated in a flow of O_2 (30 ml min^{-1}) at 873 K for ca. 1 h. Then, the reactor was evacuated at 873 K to 10^{-4} Pa for 20 min. After the vacuum treatment the temperature of the catalyst was set to the desired value (623–873 K) and an $O_2 : Ne = 1 : 1$ mixture was pulsed over the catalysts.

2.3. Catalytic testing

The catalytic tests were carried out in a fixed-bed reactor made of quartz at ambient pressure. The reactor was immersed into a bed of fluidized sand serving as a source or sink of heat. The reactant-gas stream consisted of 2–15 vol% of oxygen and 30 vol% of methane in nitrogen. The total flow rate and the reaction temperature were fixed at 60 cm^3 min^{-1} and 1023 K, respectively. For comparison of selectivities at similar degrees of methane conversion the tests were performed with different amounts of catalyst varying from 0.03 to 0.140 g. The methane conversion amounted to 9–14%. The products and reactants were analysed by using a micro gas chromatograph (Chrompack CP-2002) equipped with Poraplot Q and Molsiev 5 columns.

2.4. TAP data treatment and fitting

The parameter estimation procedure based on a numerical solution of partial differential equations which described the processes of diffusional transport, adsorption/desorption and the catalytic reaction inside the TAP reactor, was described earlier [18,20]. The program used allowed a simple implementation of different models.

3. Kinetic models

3.1. Model 1: Langmuir-type adsorption

Assuming the Langmuir model for oxygen adsorption with the rate constants k_{ads} and k_{des},

$$O_2 + z \underset{k_{des}}{\overset{k_{ads}}{\rightleftharpoons}} z\text{–}O_2 \tag{1}$$

the mass balance for the gas-phase and surface oxygen in the reactor can be written as

$$\frac{\partial C_{O_2}}{\partial t} = D_{eff}\frac{\partial^2 C_{O_2}}{\partial x^2} - C_{tot} \times \left(k_{ads}C_{O_2}(1-\Theta_{O_2}) - k_{des}\Theta_{O_2}\right), \tag{2}$$

$$\frac{\partial \Theta_{O_2}}{\partial t} = k_{ads}C_{O_2}(1-\Theta_{O_2}) - k_{des}\Theta_{O_2}, \tag{3}$$

where $1 = \Theta_{O_2} + \Theta_z$, $\Theta_{O_2} = C_{z\text{–}O_2}/C_{tot}$, $\Theta_z = C_z/C_{tot}$ and D_{eff} is the effective Knudsen diffusion coefficient.

3.2. Model 2: one-stage reversible dissociative adsorption

$$O_2 + 2z \underset{k_{des}}{\overset{k_{ads}}{\rightleftharpoons}} 2z\text{–}O \tag{4}$$

For this model, the mass balance changes to

$$\frac{\partial C_{O_2}}{\partial t} = D_{eff}\frac{\partial^2 C_{O_2}}{\partial x^2} - C_{tot}^2 \times \left(k_{ads}C_{O_2}(1-\Theta_O)^2 - k_{des}\Theta_O^2\right), \tag{5}$$

$$\frac{\partial \Theta_O}{\partial t} = 2C_{tot}\left(k_{ads}C_{O_2}(1-\Theta_O)^2 - k_{des}\Theta_O^2\right), \tag{6}$$

where $1 = \Theta_O + \Theta_z$, $\Theta_z = C_z/C_{tot}$, $\Theta_O = C_{z\text{–}O}/C_{tot}$ and D_{eff} is the effective Knudsen diffusion coefficient.

3.3. Model 3: two-stage reversible dissociative adsorption

Reversible molecular adsorption occurs as the first step; this molecular precursor undergoes further dissociation in which one more active centre of the same nature participates. This model was chosen based on experimental data [22]. In our earlier study on contact potential differences between REO- and CaO-based catalysts and a gold electrode [8,23] we have also observed the formation of adsorbed dioxygen in the form of O_2^- at temperatures up to 400 °C and of O^-/O_2^{2-}, O^{2-} at higher temperatures. The formation of peroxide ions on alkali or alkali-earth oxides have been well proven by Raman spectroscopy and charge distribution analysis [6,22]. Furthermore, a similar model was successfully used for the simulation of oxygen adsorption under OCM conditions [24]. The model and mass balance for data evaluation can be written as follows:

$$O_2 + z \underset{k_{des}}{\overset{k_{ads}}{\rightleftharpoons}} z\text{–}O_2 \tag{7}$$

$$z\text{–}O_2 + z \underset{k_{ass}}{\overset{k_{dis}}{\rightleftharpoons}} 2z\text{–}O \tag{8}$$

$$\frac{\partial C_{O_2}}{\partial t} = D_{eff}\frac{\partial^2 C_{O_2}}{\partial x^2} - C_{tot} \times \left(k_{ads}C_{O_2}(1-\Theta_O-\Theta_{O_2}) - k_{des}\Theta_{O_2}\right), \tag{9}$$

$$\frac{\partial \Theta_{O_2}}{\partial t} = k_{ads}C_{O_2}(1-\Theta_{O_2}-\Theta_O) - k_{des}\Theta_{O_2} - C_{tot}\left(k_{dis}\Theta_{O_2}(1-\Theta_{O_2}-\Theta_O) - k_{ass}\Theta_O^2\right), \tag{10}$$

$$\frac{\partial \Theta_O}{\partial t} = 2C_{tot}\left(k_{dis}\Theta_{O_2}(1-\Theta_{O_2}-\Theta_O) - k_{ass}\Theta_O^2\right), \tag{11}$$

where $1 = \Theta_O + \Theta_{O_2} + \Theta_z$, $\Theta_{O_2} = C_{z\text{–}O_2}/C_{tot}$, $\Theta_z = C_z/C_{tot}$, $\Theta_O = C_{z\text{–}O}/C_{tot}$ and D_{eff} is the effective Knudsen diffusion coefficient.

4. Results and discussion

4.1. Model discrimination and parameter estimation

The experimental transient oxygen responses for all the catalysts studied at 873 K are presented in figure 1. One can see that these responses differ significantly in their form. As the transport characteristics influence the response signal, it is necessary to determine the regime of gas diffusion through the reactor. The simplest method proposed by

Notation

C_{O_2}	gas-phase oxygen concentration (mol m^{-3})
C_{z-O_2}	concentration of molecular adsorbed oxygen species (mol m^{-3})
C_{z-O}	concentration of atomic adsorbed oxygen species (mol m^{-3})
C_{tot}	total concentration of adsorption sites (mol m^{-3})
D_{eff}	effective Knudsen diffusion coefficient (m^2 s^{-1})
d_p	catalyst particle size (μm)
E_a	activation energy (kJ mol^{-1})
F_{Ne}	flow of neon at the reactor outlet (mol s^{-1})
H_p	peak height of the normalised neon flow, F_{Ne}/N_{pNe} (s^{-1})
k_{ads}	adsorption rate constant (m^3 mol^{-1} s^{-1})
k_{des}	desorption rate constant (s^{-1})
k_{dis}	dissociation rate constant (m^3 mol^{-1} s^{-1}) – model 3
k_{ass}	association rate constant (m^3 mol^{-1} s^{-1}) – model 3
k_0	pre-exponential factors (s^{-1} and m^3 mol^{-1} s^{-1} for reactions of 1st and 2st order, respectively)
Θ_{O_2}	fractional coverage of molecular adsorbed oxygen (dimensionless)
Θ_O	fractional coverage of atomic adsorbed oxygen (dimensionless)
Θ_z	fractional coverage of free adsorption sites (dimensionless)
t	time (s)
t_p	time of a maximum exit flow of neon (s)
T	temperature (K)
x	reactor coordinate (m)

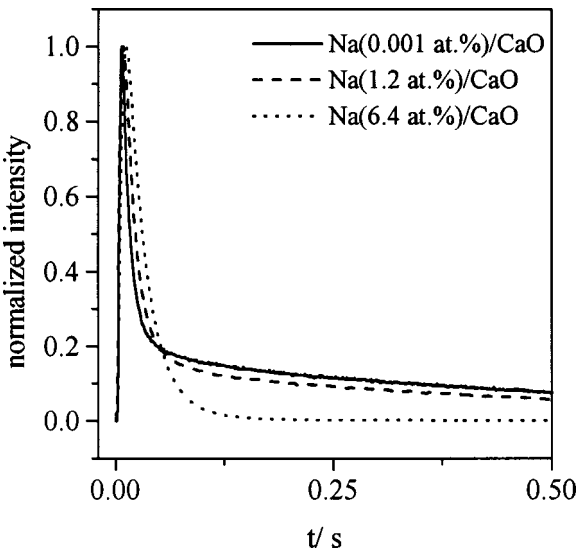

Figure 1. Transient responses of oxygen when pulsing on O_2–Ne mixture over different catalysts at 873 K.

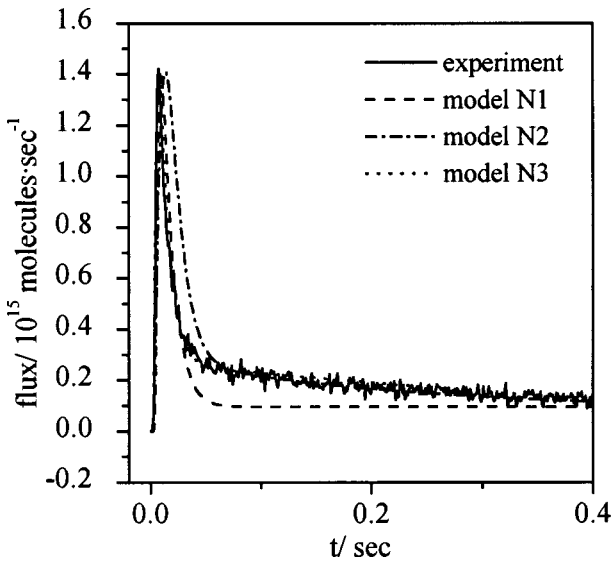

Figure 2. Comparison between models 1–3 and experimental responses of oxygen over Na(0.001 at%)/CaO at 873 K.

Gleaves et al. [21] for the verification of the TAP-2 system is the check of the following criterion:

$$H_p t_p \leqslant 0.31, \tag{12}$$

where H_p is the peak height of the normalised neon flow, F_{Ne}/N_{pNe} (s^{-1}), t_p is the time of a maximum exit flow of neon (s).

The values of $H_p t_p$ obtained for all the catalysts at different temperatures ranged between 0.27 and 0.31. Thus, these results verify that all the pulse experiments were performed in the Knudsen diffusion regime.

In the following, the results of numerical fitting of the experimental data for oxygen adsorption are described. Three different models described in section 2 were used for fitting the measured responses at the reference temperature 873 K. The search of parameters was performed in a wide range of possible values for the rate constant and adsorption sites (10^{-4}–10^6) using genetic and simplex algorithms implemented in the software applied. As the results of this modelling no adequate description was achieved when using models 1 and 2, thus no set of parameters was found to fit the measured responses in this case. The best fitting of experimental data at a reference temperature was obtained by model 3. This was valid for all the catalysts studied. The fit of the different models is illustrated for one catalyst (Na(0.001 at%)/CaO) in figure 2. It is necessary to note that a correlation between the three parameters (C_{tot}, k_{ads}, k_{dis}) was found. Therefore, only the effective rate constants, which contain the total concentration of active sites ($k_{ads}^{eff} = C_{tot} k_{ads}$ and $k_{dis}^{eff} = C_{tot} k_{dis}$), were determined.

Based on the results on model discrimination at the reference temperature model 3 was selected to describe the transient responses at other temperatures. In this case activation energies for four reaction steps (adsorption, desorption, dissociation, association) were derived according to equation (13):

$$k_{T_i} = k_{T_{\text{ref}}} \exp\left(-\frac{E_a}{R}\left(\frac{1}{T_i} - \frac{1}{T_{\text{ref}}}\right)\right). \qquad (13)$$

The simulated and experimental responses at different temperatures for Na(6.4 at%)/CaO are presented in figure 3. A good description of the transient data is obtained at each temperature. This is valid for all the catalysts studied. Kinetic parameters obtained for different catalysts assuming model 3 are summarised in table 1.

4.2. Influence of catalyst composition on kinetic data and surface coverages

The kinetic data obtained are discussed in the terms of the relationship between the catalyst composition and the kinetics of oxygen interaction. As the results presented in table 1 show, the addition of an alkali promoter into CaO influences significantly the activation energies of desorption and dissociation of molecular adsorbed oxygen. It was also found that alkali doping influenced the ratio of $k_{\text{ads}}/k_{\text{dis}}$ (figure 4). It decreased with increasing sodium concentration. The ratio of $k_{\text{ads}}/k_{\text{dis}}$ can indicate the ability of the catalyst for converting molecular adsorbed oxygen species to atomic adsorbed oxygen species. This assumption can be proved by estimating the coverage of the catalyst surface by adsorbed species from the simulation of the experimental responses of oxygen. Temporal and spatial profiles of Θ_{O_2} and Θ_O for Na(6.4 at%)/CaO under TAP conditions are shown in figure 5. The coverages with molecular adsorbed species passes through a maximum with time and decreases with the length of the catalyst bed. The formation of atomic species rose up to a constant value with the time and decreased within the catalyst bed. It was found that the ratio of Θ_O/Θ_{O_2} increases with an increase of sodium concentration for all Na_2O/CaO catalysts. Comparing the ratio of $k_{\text{ads}}/k_{\text{dis}}$ with the ratio of Θ_O/Θ_{O_2} it is possible to conclude that the lower the ratio of $k_{\text{ads}}/k_{\text{dis}}$ is the higher the ratio of Θ_O/Θ_{O_2} becomes. This means that the coverage of the catalyst surface by different oxygen species depends on the ratio of $k_{\text{ads}}/k_{\text{dis}}$. Increasing the ratio of Θ_O/Θ_{O_2} with an increase of sodium concentration is explained by formation of additional anion vacancies within the Ca sublattice due to Na incorporation. The anion vacancies promote the dissociation of molecular adsorbed oxygen according to equation (8). From our earlier study on the total conductivity and the contact potential difference (CPD) [23] we concluded that the incorporation of sodium into the cation sublattice of CaO increased the conversion of molecular adsorbed oxygen into atomic surface species because of the formation of additional anion vacancies.

Thus, from the simulation of the experimental data it is possible to conclude that the mechanism of oxygen in-

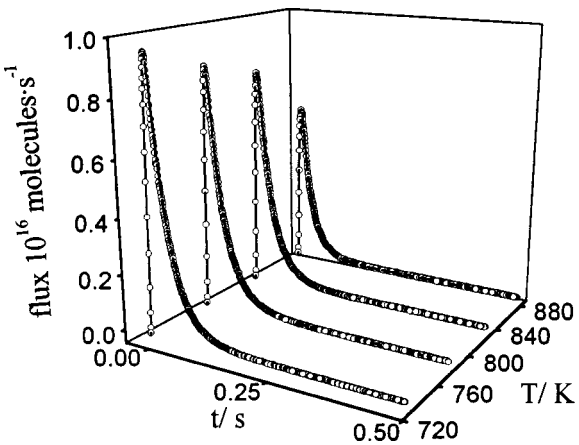

Figure 3. Comparison between simulated (model 3) and experimental (circles) responses of oxygen over Na(6.4 at%)/CaO at different temperatures.

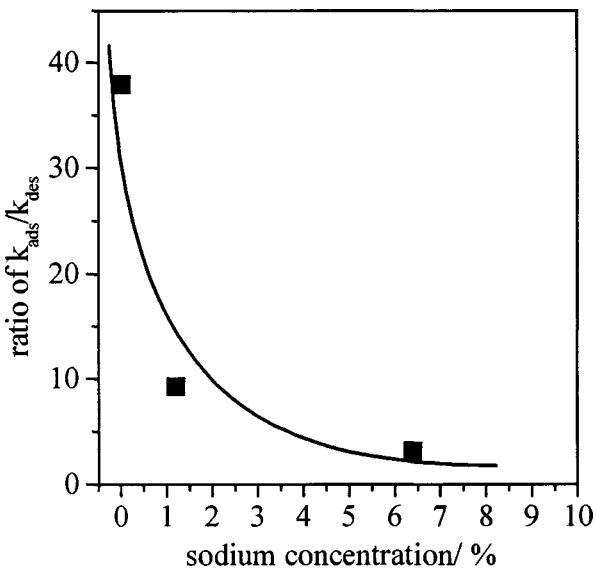

Figure 4. Ratio of $k_{\text{ads}}/k_{\text{dis}}$ versus concentration of sodium promoter ($T = 1023$ K).

Table 1
Transient kinetic parameters for the elementary steps of oxygen interaction with different catalysts assuming model 3.

	$k_{\text{ads}}^{\text{eff}}$		k_{des}		$k_{\text{dis}}^{\text{eff}}$		k_{ass}	
	k_0^{eff}	E_a (kJ mol^{-1})	k_0	E_a (kJ mol^{-1})	k_0^{eff}	E_a (kJ mol^{-1})	k_0	E_a (kJ mol^{-1})
Na(0.001 at%)/CaO	9.1×10^8	89	6.6×10^7	116	1.5×10^{17}	249	2.3×10^{21}	420
Na(1.2 at%)/CaO	2.1×10^7	70	6.5×10^8	106	3.9×10^7	94	1.9×10^{16}	292
Na(6.4 at%)/CaO	8.6×10^6	80	1.6×10^5	67	8×10^6	88	6.5×10^{13}	253

teraction with the catalysts studied changes due to the incorporation of sodium cations into the cation sublattice of CaO.

4.3. Oxidative coupling of methane and oxygen adsorption

The results of oxygen simulation are discussed to explain the catalytic performances of Na_2O/CaO catalysts for the oxidative coupling of methane (OCM). The catalytic data of the catalysts studied are presented in table 2. The selectivity of C_2-products formation increases with increasing sodium concentration and decreasing oxygen partial pressure. The results obtained agree well with results published elsewhere [25–27]. When comparing the transient kinetic data on oxygen adsorption with catalytic performances in OCM a relationship between the ratio of k_{ads}/k_{dis} and C_2 selectivity (figure 6) was found. As it follows from the results on fitting the oxygen transient responses (see section 4.2), the ratio of k_{ads}/k_{dis} determines the ability of the catalysts for converting molecular adsorbed oxygen to atomic species under transient conditions. Using the Maple V programme [28], the steady-state concentrations of molecular adsorbed and atomic adsorbed oxygen were calculated from the set of algebraic equations (9), (10) and mass balance equation ($1 = \Theta_O + \Theta_{O_2} + \Theta_z$). The dependence of these concentrations on oxygen partial pressure is presented in figure 7. The ratio of Θ_O/Θ_{O_2} rises with increasing the sodium concentration and decreases with increasing oxygen partial pressure. The high coverage by molecular adsorbed oxygen may be explained by stabilisation of peroxides on the catalyst surface. Peroxides of alkali/alkali-earth metals can be stabilised at high temperatures at high oxygen pressures [6,22,29]. It should be also noted that there is no incorporation of adsorbed surface species into the catalyst volume in model 3. Therefore it can lead to a decrease of the surface coverage by molecular adsorbed oxygen. Figure 8 presents the selectivity of C_2-products formation over all Na_2O/CaO catalysts at different oxygen partial pressures versus the ratio of Θ_O/Θ_{O_2} estimated at the same oxygen partial pressures as in the catalytic runs. From the results presented it follows that the selectivity obtained grows with increasing the ratio of Θ_O/Θ_{O_2}. This means that the high

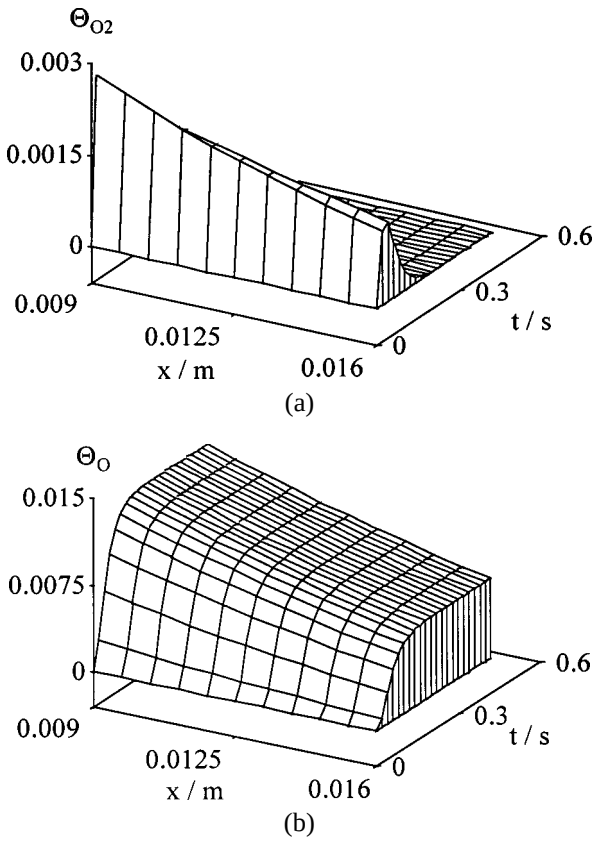

Figure 5. Temporal and spatial profiles of the surface coverage by molecular (a) and atomic (b) adsorbed oxygen species during a pulse experiment ($T = 873$ K, Na(6.4 at%)/CaO).

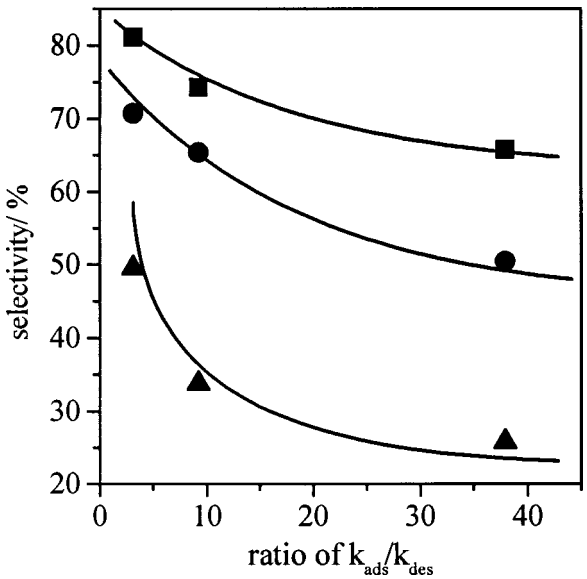

Figure 6. Selectivity of C_2 products versus the ratio of k_{ads}/k_{dis} ($T = 1023$ K): (•) 2 kPa oxygen partial pressure, (■) 5 kPa oxygen partial pressure and (▲) 15 kPa oxygen partial pressure.

Table 2
Selectivity of formation of OCM products over Na_2O/CaO catalysts at various oxygen concentrations. Concentration of methane was constant (30 vol%), $T = 1023$ K.

$p(O_2)$ (vol%)	Selectivity (%)								
	Na(0.001 at%)/CaO			Na(1.2 at%)/CaO			Na(6.4 at%)/CaO		
	C_2	CO	CO_2	C_2	CO	CO_2	C_2	CO	CO_2
2	65.8	17.2	17.0	74.3	7.6	18.1	81.1	3.5	15.4
5	50.4	23.3	26.3	65.4	4.1	30.5	70.8	5.0	24.2
15	25.8	14.9	59.3	33.8	7.6	58.6	49.5	5.1	45.4

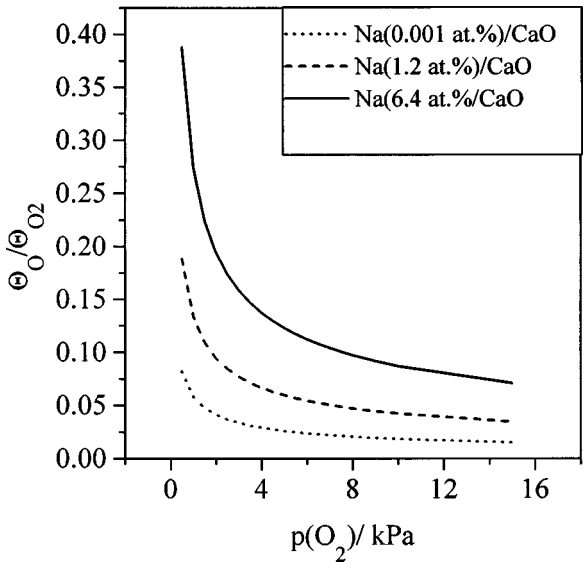

Figure 7. Steady-state ratio of Θ_O/Θ_{O_2} simulated for Na_2O/CaO catalysts versus oxygen partial pressure without presence of methane.

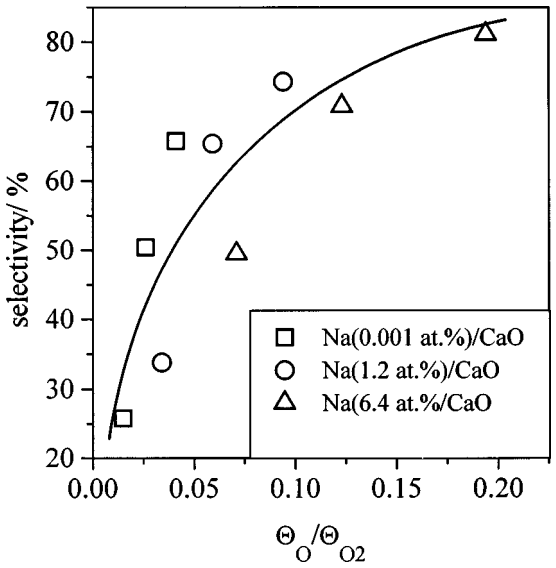

Figure 8. Selectivity of C_2-products formation over Na_2O/CaO catalysts versus steady-state ratio of Θ_O/Θ_{O_2} simulated at oxygen partial pressures without presence of methane.

selectivity of C_2-products formation can be achieved by reducing the concentration of adsorbed molecular oxygen. The increase of the C_2-products selectivity with decreasing concentration of adsorbed molecular oxygen species can be due to the fact that the oxygen species consisting of more than one oxygen atom promote especially C–C bond cleavage [30]. This reaction is probably the initial step of C_2-products combustion. The positive effect of the transformation of molecular oxygen in atomic oxygen surface species on OCM selectivity was previously found in our works [8,23,31,32].

Thus, the addition of an alkali dopant into the CaO lattice influences the process of oxygen activation due to decreasing the ratio of k_{ads}/k_{dis} which, in turn, results in reducing the coverage of the surface with molecular oxygen species and, hence, in high selectivity for C_2-products formation.

5. Conclusions

Modelling of transport and sorption processes within the TAP reactor was applied to fit the oxygen transient responses obtained at diffrent temperatures (623–873 K) over Na_2O/CaO catalysts. Three different adsorption models were tested. A good description of all the transient data was achieved assuming the two-stage reversible dissociative adsorption via a molecular precursor. The kinetic constants were correlated with temperature according to the Arrhenius law to determine apparent activation energies for the various surface processes. For Na_2O/CaO catalysts it was established that the ratio of k_{ads}/k_{dis} decreases with increasing sodium concentration. This ratio determines the coverage of a catalyst surface with both atomic and molecular oxygen. The lower the ratio of k_{ads}/k_{dis} is, the higher the ratio of Θ_O/Θ_{O_2} becomes. A correlation between the ratio of Θ_O/Θ_{O_2} and selectivity of C_2-products formation for OCM was found. Decreasing concentration of molecular adsorbed oxygen due to increasing the rate of its dissociation improves the catalytic performances of Na_2O/CaO catalysts with increasing sodium concentration.

Acknowledgement

This work was supported by the German Federal Ministry for Education and Research (Contract No. 03C30120) and by the State of Berlin. EVK thanks Alexander von Humboldt Foundation for a postdoctoral fellowship allowing him to work at the Institut für Angewandte Chemie Berlin-Adlershof e.V.

References

[1] G.K. Boreskov, in: *Catalysis: Science and Technology*, eds. J. Andersen and M. Boudart (Springer, Berlin, 1982) p. 40.
[2] A. Belansky and J. Haber, *Oxygen in Catalysis* (Dekker, New York, 1996).
[3] V.D. Sokolovskii and A.E. Mamedov, Catal. Today 14 (1992) 331.
[4] H.H. Kung, Adv. Catal. 40 (1994) 1.
[5] G.W. Keulks, N. Liao, W. An and D. Li, in: *Proc. of the 10th Int. Congress on Catalysis*, 19–24 July 1992 (1993) p. 2253.
[6] G. Mestl, H. Knözinger and J.H. Lunsford, Ber. Bunsenges. Phys. Chem. 97 (1993) 319.
[7] J.X. Wang and J.H. Lunsford, J. Phys. Chem. 90 (1986) 5883.
[8] G. Gayko, D. Wolf, E.V. Kondratenko and M. Baerns, J. Catal. 178 (1998) 441.
[9] Z. Kalenik and E.E. Wolf, Catal. Lett. 9 (1991) 441.
[10] J.T. Gleaves, J.R. Ebner and T.C. Kuechler, Catal. Rev. Sci. Eng. 30 (1988) 49.
[11] J.T. Gleaves and G. Genti, Catal. Today 16 (1993) 69.
[12] O.V. Buyevskaya, M. Rothaemel, M. Zanthoff and M. Baerns, J. Catal. 150 (1994) 71.
[13] E.P.J. Mallens, J.H.B.J. Hoebink and G.B. Marin, Catal. Lett. 33 (1995) 291.

[14] O.V. Buyevskaya, K. Walter, D. Wolf and M. Baerns, Catal. Lett. 38 (1996) 81.
[15] G.D. Svoboda, J.T. Gleaves and P.L. Mills, Ind. Eng. Chem. Res. 31 (1992) 19.
[16] B. Zou, M.P. Dudukovic and P.L. Mills, J. Catal. 145 (1994) 683.
[17] G. Creten, S. Lafyatis and G.F. Froment, J. Catal 154 (1995) 151.
[18] M. Rothaemel and M. Baerns, Ind. Eng. Chem. Res. 35 (1996) 1556.
[19] M. Soick, O. Buyevskaya, M. Höhenberger and D. Wolf, Catal. Today 32 (1996) 163.
[20] M. Soick, D. Wolf and M. Baerns, Chem. Eng. Sci., submitted.
[21] J.T. Gleaves, G.S. Yablonskii, P. Phanawadee and Y. Schuurman, Appl. Catal. 160 (1997) 55.
[22] F. Freund, G.C. Maiti, F. Batllo and M. Baerns, J. Chim. Phys. 87 (1990).
[23] E.V. Kondratenko, M. Baerns and D. Wolf, Catal. Lett. 58 (1999) 217.
[24] D. Wolf, Catal. Lett. 27 (1994) 207.
[25] K. Otsuka, A.A. Said, K. Jinno and T. Komatsu, Chem. Lett. 1 (1987) 77.
[26] A.G. Anshits, N.P. Kirik, V.G. Roguleva, A.N. Shigapov and G.E. Selyutin, Catal. Today 4 (1989) 399.
[27] T. Grzybeck and M. Baerns, J. Catal. 129 (1991) 106.
[28] Maple V, Release 5, Waterloo Maple Inc.
[29] I.I. Vol'nov, *Peroxides, Hyperoxides and Ozonides of Alkali and Alkali Earth Metals* (Plenum, New York, 1966).
[30] M. Iwamoto and J.-H. Lunsford, J. Phys. Chem. 84 (1980) 3079.
[31] H. Borchert and M. Baerns, J. Catal. 168 (1997) 315.
[32] D. Wolf, M. Slinko, E. Kurkina and M. Baerns, Appl. Catal. 166 (1998) 47.